

Analysis of a Hybrid Molten Carbonate Fuel Cell and Gas Turbine Cycle

Elisângela Martins Leal¹, Barbara Emanuelle Sanches Silva²,
Amauri Menezes Leal Junior³

^{1,2}Department of Mechanical Engineering, School of Mining, Brazilian Federal University of Ouro Preto, Campus Morro do Cruzeiro S/N, Bauxita, Ouro Preto, Minas Gerais, Brazil. ZIP: 35.400-000

³Network in Materials Engineering (REDEMAT), Department of Metallurgical and Materials Engineering, School of Mining, Brazilian Federal University of Ouro Preto, Campus Morro do Cruzeiro S/N, Bauxita, Ouro Preto, Minas Gerais, Brazil. ZIP: 35.400-000

Received 26 February 2020; Accepted 09 March 2020

Abstract:

Background: Hybrid systems with fuel cells and thermal engines are studied with promising results. Molten carbonate fuel cells (MCFC) show many advantages compatible with the current demands for energy production in a sustainable competitive way.

Materials and Methods: This paper focuses on the computational investigation of an indirect internal reforming MCFC coupled to a gas turbine (GT) system. The technical analysis comprises of energy analysis of the hybrid cycle, using the Gibbs function minimization technique for the methane steam reforming process. The assessment is performed to determine the influence of the hybrid cycle operating temperature and pressure, steam-to-carbon ratio, and fuel and oxidant usage in the fuel cell.

Results: Results show that the increase in temperature and in operating pressure of the fuel cell and the fuel reform rate improves the hybrid system performance. Variation in the utilization factor, however, did not determine an expressive increase in system efficiency. For the same fuel mass flow rate, it is possible to see that the variation in the operating temperature of the fuel cell resulted in an increase in the total power of the hybrid system when compared to the results of the pressure increase. The increase in temperature resulted in a maximum increase of 12% in delivered power and corresponding to about 7% system efficiency increase. Instead, an increase in pressure of about 4% corresponding to an increase of about 2% system efficiency.

Conclusion: Although an increase in the fuel cell's power density was observed for the same mass flow rate in the system, the pressure negatively influenced the total delivered power by the fuel cell.

Keyword: Molten carbonate fuel cell; gas turbine; hybrid system; energy analysis

I. INTRODUCTION

According to the Global Energy Statistical Yearbook [1], the contribution of BRICS (Brazil, Russia, India, China, and South Africa) countries to the electricity consumption had an increase of 72% between 2010 and 2018. In these years, after a period of stagnation until 2016, energy-related carbon dioxide emissions grew by 2.1% in 2017 and by 1.9% in 2018. Nevertheless, the increase in energy demand associated with the urgency for the reduction of pollutant emission drives the need for alternatives to energy systems production. Renewable energy is still a challenge due to its installation cost and local dependence of the source, the optimization of the energy generation processes justifies the efforts of this researches.

One of the ways to reduce the fossil fuel impact on the atmosphere is through more efficient energy generation systems, such as combined cycles. According to Dincer et al. [2], power generation systems with lower greenhouse gases (GHG) emissions are being considered or installed globally to reduce GHG emissions. The benefit of this combination is the better use of fuel, which is, more power can be produced from the same amount of fuel, increasing the system efficiency and lowering the release of pollutants per kilowatt-hour generated.

Hauschild [3] defines a hybrid system like the one formed by two or more sources of energy production working together to meet the demand of a common consumer and this has been observed has an important alternative for the optimization of energy generation processes. Fuel cell hybrid systems have been described to meet efficiencies of about 80% LHV base when using natural gas promoting pollutant emissions reduction [4]. The possibility to combine technologies that use different mechanisms of energy generation is the main aspect studied in these systems. Thus, starting from the same primary source, the energy potential not used in the energy generation by one technology might be used by the other, increasing net efficiency. This principle leads to the proposition of hybrid cycles using fuel cells and thermal engines since 1989 [5].

The fuel cell produces electrical energy through oxy-fuel reduction reactions presenting a non-limitation due to the irreversibility of combustion reactions and its energy production efficiency [6, 7]. High-temperature fuel cells also have the advantage of promoting the use of CO₂ [8] and the flexibility of fuel use by internal reforming and gasification of energy sources such as coal and biomass [9-12]. The use of thermal engines within the hybrid cycle is aimed at harnessing the heat generated to produce electricity, considering that in this type of fuel cell almost half of the energy from the fuel is lost in the form of heat.

Marefati and Mehrpooya [13] studied a cogeneration system using a molten carbonate fuel cell (MCFC). The authors found high overall efficiency (around 65%) and a total exergy efficiency gain of 0.12%. Marefati et al. [14] also studied a cogeneration system using an MCFC and a solar collector to investigate a carbon capture process. The hybrid system produced around 720 MW of electrical power with a 71% overall efficiency power plant. Mehrpooya et al. [15] evaluated a power generation process using an MCFC hybrid system, oxy-fuel, Rankine cycle, and solar parabolic thermal energy. The integrated structure showed an overall thermal efficiency of about 73% and total exergy efficiency of almost 63%. In addition, Mahmoudi et al [16] analyzed an MCFC combined cycle using the Organic Rankine cycle (ORC). The best performance was achieved using toluene and n-pentane in the ORC, obtaining about 68% of exergy efficiency and 32 US\$/GJ as the lowest power unit cost. The literature has been demonstrated the study of an MCFC in hybrid systems using various technologies and using many approaches [17-39].

Hybrid systems with solid oxide [40] and molten carbonate fuel cells [41] were successfully demonstrated in the sub-MW size class and reached efficiencies of 53% and 56%, PCI base, respectively. McLarty et al. [4], however, described another system involving an MCFC associated with a micro gas turbine achieving an efficiency of 74.4%, PCI base. MCFCs alone have been registered to achieve efficiencies of 48% [42].

The steady-state of the MCFC energy production system has been studied under various parameters such as pressure profile, temperature distribution, electric efficiency or fuel usage [43-45]. However, its behavior in a hybrid system is still explored. A unified hybrid fuel cell and thermal engine model was demonstrated by Zhang et al. [46] reproducing important results of the literature. Some limiting aspects such as production cost and durability, especially in fuel cells, however, represent an important challenge for the diffusion of these systems [47].

Regarding the gas turbine unit (GTU), Pashchenko [48] determined the optimal operational parameters of a GTU with the thermochemical exhaust heat recuperation system by using steam methane reforming. In his paper, the influence of temperature, pressure, and inlet reaction mixture composition on the recuperation rate were determined to show that for the temperature range of 900 K to 1000 K, operating pressure less than 10 bar, the recuperation rate reaches a maximum value for the steam-to-carbon ratio of two.

This study aims to analyze technically a hybrid system consisted of a molten carbonate fuel cell and a gas turbine, through the evaluation of the main variables on the efficiency and power generation of the hybrid system. Thus, it will be possible to find fuel cell design points and work in them. Initially, it is demonstrated how operation limits of the molten carbonate fuel cell at the design point influence in the energy production of the device. Afterward, an analysis of the fuel cell/gas turbine hybrid cycle was accomplished using MS Excel software, including the model validation with the comparison between the results of the fuel cell / hybrid system model and those available in the literature.

II. DESCRIPTION AND MATHEMATICAL MODELING OF THE HYBRID SYSTEM

Hybrid fuel cell/gas turbine systems show potential for high efficiency, low pollutant emissions, fuel flexibility and dynamic responsiveness [40,49]. Experimental and theoretical analyses of such hybrid systems confirm this potential. Besides, the construction of the sites might be fast and with minimal environmental impact.

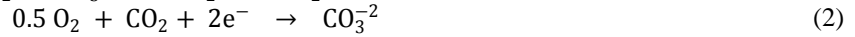
Molten Carbonate Fuel Cell (MCFC)

High-temperature fuel cells composed of a molten carbonate salt mixture electrolyte suspended in a porous, chemically inert ceramic matrix are defined as molten carbonate fuel cells (MCFC). It is especially applicable in stationary processes among the types of fuel cells currently available due to the operating temperature of the fuel cell around 923.15 K, which is enough for the electrochemical conversion processes without the need for noble metals catalysts. Yu et al. [50] highlight that many projects using MCFCs have shown the great commercial value of fuel cells in the application fields of independent power sources including the MW-scale MCFC power plant [51] and the U.S. distributed generation fuel cell program [52]. Between 2012 and 2013, the power delivered by MCFCs around the world rose from 62.0 to 91.9 MW/year, an increase of 48.2% [53].

The reforming reaction of conventional fuels is also favored by the high temperature of fuel cells. It allows the reaction to be realized internally in the own cell, simplifying the system and increase the overall

efficiency since the energy used for the reforming processes comes from the heat generated in the cell itself. MCFCs also have the advantage to be able to use CO and CO₂ in the electrochemical and reforming reactions, which increase the range of fuels that can be used in the process [54].

The anode, cathode and overall reactions in MCFC are, respectively [6]:



Knowing the equilibrium potential (E_{eq}) of the cell and the irreversible losses (V_{cat} and V_{an}) of the process is possible to calculate the operational cell voltage (E) of the fuel cell based on Nernst equation when the current density (j) is defined [55,56]:

$$E = E_{eq} + j(R_t + V_{an} + V_{cat}) \quad (4)$$

$$E_{eq} = E^0 + \frac{R_g T}{2 F_n} \ln \left(\frac{p_{\text{H}_2} p_{\text{O}_2}^{0.5} p_{\text{CO}_{2,cat}}}{p_{\text{H}_2\text{O}} p_{\text{CO}_{2,an}}} \right) \quad (5)$$

$$E^0 = \frac{R_g T}{2 F_n} \ln(K_0) \quad (6)$$

$$K_0 = \exp \left(\frac{-\Delta G_r}{R_g T} \right) \quad (7)$$

$$R_t = \delta \left\{ a \cdot \exp \left[b \left(\frac{1}{T} - \frac{1}{T_0} \right) \right] \right\} \quad (8)$$

Where: E is the working cell voltage (V); V_{an} and V_{cat} is the irreversible losses at the anode ($\Omega \cdot \text{m}^2$) and cathode ($\Omega \cdot \text{m}^2$), respectively; R_g is the universal gas constant (8.314 kJ/kmol.K); F_n is the Faraday constant (96487.309 C/mol); T is the cell temperature (K); p_{H_2} , p_{O_2} and $p_{\text{CO}_{2,cat}}$ are the partial pressure of hydrogen, oxygen and carbon dioxide at the cathode, respectively; $p_{\text{H}_2\text{O}}$ and $p_{\text{CO}_{2,an}}$ are the partial pressure of water and carbon dioxide at the anode, respectively; K_0 is the reaction equilibrium constant [-]; ΔG_r is the Gibbs free energy of the fuel cell reaction [kJ/kmol] (Eq. 3); T_0 is the reference temperature [K].

The total resistance (R_t) is related to the cell building material since δ is the equivalent thickness of the diffusion layer, a and b are constants related to the fuel cell materials. Calculation of the equilibrium potential predicts that increasing the operating pressure of the fuel cell results in increased partial pressures of the reactants, the solubility and mass transport rates. However, an excessive increase in the operating pressure will favor the carbon deposition (Boudouard reaction) and suppress the reforming of methane to form H₂ by the Le Chatelier principle, reducing the gas flow and the fuel availability for the reaction, respectively [6].

Regarding the effect of cell pressure, Eq. (3) shows that a transfer of CO₂ from the cathode gas stream to the anode gas stream must occur for electricity production from the MCFC. Thus, it is assumed that when the partial pressures of CO₂ are identical at the anode and cathode, the cell potential will depend on the partial pressures of hydrogen, oxygen, and water. However, in real systems, the partial pressures of CO₂ are different at the anode and at the cathode, so the cell potential is affected accordingly. Besides, an increase in the MCFC operating pressure can result in increased cathode corrosion. Corrosion of the cathode is related to the acidity of the electrolyte. An increase in the cell pressure (consequently, an increase in the partial pressure of CO₂) can accelerate the corrosion process and nickel precipitation, causing the fuel cell to fail. Therefore, the proper choice of operating pressure of the MCFC cell is necessary and has a direct relationship with the useful life, cost, and feasibility of the device [7].

Polarization in the electrodes as demonstrated by Selman and Lin [57] can be obtained, regarding the irreversible losses (V_{cat} and V_{an}) of the process, by:

$$V_{an} = 2.27 \cdot 10^{-9} (p_{\text{H}_2})^{-0.42} (p_{\text{CO}_2})^{-0.17} (p_{\text{H}_2\text{O}})^{-1.00} \exp \left[\frac{53500}{R_g} \left(\frac{1}{T_0} - \frac{1}{T} \right) \right] \quad (9)$$

$$V_{cat} = 7.51 \cdot 10^{-10} (p_{\text{O}_2})^{-0.43} (p_{\text{CO}_2})^{-0.09} \exp \left[\frac{53500}{R_g} \left(\frac{1}{T_0} - \frac{1}{T} \right) \right] \quad (10)$$

Zhang et al. [46] highlight that the ohmic polarization occurs due to the resistance of both the carbonate ions flows in the electrolyte and the electron in the electrodes and interconnectors. An energy barrier that the reagents must overcome for the reaction to occur defines activation polarization. On the other hand, the difference between the rate of diffusion of the reactant gases by the electrodes and the reaction rate leads to the concentration polarization results. Polarization resistance shows an explicit dependence on reactants' partial pressures (p) on each electrode, reference temperature (T_0) and the operating temperature of the cell (T). Reference temperature for MCFCs is described as 923.15K [58]. The partial pressures are defined by gas compositions and operating pressure. Therefore, it is necessary to evaluate the influence of these parameters in the hybrid system to analyze the best relationship among them.

In this study, chemical equilibrium was used to calculate the gas concentrations required in the determination of the anode and cathode resistances as well as for the results of fuel reforming and gas shift reactions. The values of the equilibrium constants at different fuel cell temperature and pressure conditions were also calculated.

Finally, the electric energy density produced by the fuel cell can be calculated as [56]:

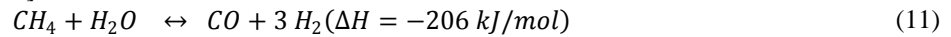
$$W_{FC} = E \cdot j \quad (11)$$

Where: W_{FC} is the fuel cell power density produced [$\text{kW}\cdot\text{m}^{-2}$], E is the operational cell voltage [V] and j is the current density [$\text{A}\cdot\text{m}^{-2}$].

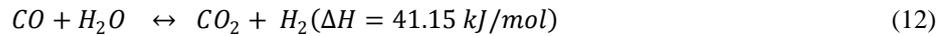
Hybrid system simulation

According to Wee [59], in the MCFC, the mainly anode products are carbon dioxide and steam. Unreacted fuel and carbon monoxide can also be found in the anode products at a low-level and they can be used as fuel for extra power generation in the gas turbine. According to the literature [60-66]; theoretical overall efficiency of the hybrid system consisting of a molten carbonate fuel cell and a gas turbine ranges from 75 to 80%, including operation in cogeneration systems. Grillo et al. [67], and Lobachyov and Richter [65] state that, even considering losses, the system can reach efficiencies higher than 60%.

This work considers an indirect internal reforming process. Due to the availability and current usage status of this source, pure methane gas was chosen as the fuel to be reformed for hydrogen production, which reaction is described as [59]:



In addition, the shifting reaction occurs [59]:



In theory, every mole of methane produces four moles of hydrogen. The reactions are in chemical equilibrium. In the study of Xu and Froment [68], the reforming and shifting reactions are dependent on the temperature and can be expressed as:

$$\log(Kp) = k_1 T^4 + k_2 T^3 + k_3 T^2 + k_4 T + k_5 \quad (13)$$

Where: Kp is the equilibrium constant of the reactions (Eq. 11 and 12), and k_j to k_5 are experimental constants, shown in Table 1.

Table no1. Constants for the reforming and shifting reactions [68,69].

Constant	Reforming reaction	Shifting reactions
k_1	-2.63121×10^{-11}	5.47301×10^{-12}
k_2	1.24065×10^{-7}	-2.57479×10^{-8}
k_3	-2.25232×10^{-4}	4.63742×10^{-5}
k_4	0.195028	-0.03915
k_5	-66.13950	13.20970

Assuming that the reforming and shifting reactions were always in equilibrium, the equilibrium constants can also be calculated as a function of the reactants partial pressures of the reactions 11 and 12 [70]:

$$Kp_{reform} = p_{\text{H}_2}^3 p_{\text{CO}} (p_{\text{CH}_4} p_{\text{H}_2\text{O}})^{-1} \quad (14)$$

$$Kp_{shift} = p_{\text{H}_2} p_{\text{CO}_2} (p_{\text{CO}} p_{\text{H}_2\text{O}})^{-1} \quad (15)$$

Pashchenko [71] performed a thermodynamic analysis of the thermochemical recovery (TCR) steam methane (SMR) reforming process using the Gibbs free energy minimization technique and determined the effects that operating parameters had on process efficiency. The parameters investigated were pressure, steam-to-carbon ratio, and temperature. The results showed that the ideal operating conditions for the process with TCR were for the steam-to-carbon ratio of 2, flue gas temperature of 900-1100K and pressure below 10 bar. For a higher temperature (1200 K), the ideal steam-to-carbon ratio was 1 with operating pressures between 5 and 10 bar. Another analysis performed by Pashchenko [72] was on a compact fixed bed reactor filled with a porous Ni-Al₂O₃ catalyst in different forms. The analysis was theoretical (ANSYS Fluent) and experimental. The experimental and theoretical results showed an average error of less than 8% and the dependence of the pressure loss for the different depths of the catalyst bed is about linear. An experimental investigation conducted by Pashchenko [73] of methane reforming on the NiO-Al₂O₃ catalyst was performed to understand the effects of operating parameters (temperature, pressure, residence time and input gas composition) on the efficiency of the operation. The pressure from 1 to 5 bar has a negligible effect on methane conversion, and the addition of steam increases methane conversion, especially in the range of 500 to 800°C.

Two steam to carbon ratio (2.0 and 3.0) were assumed in the analyses. For the fuel cell, this work analyzed a temperature range of 773.15 K to 973.15 K and the pressure range from 1 to 6 atm to see the influence of each variable in the system. Furthermore, the partial pressure was obtained based on the average

molar concentrations of the fluid components at the inlet and outlet of each electrode, so that the fuel utilization rate ($U_{f_{an}}$) in the anode was also a parameter to be considered and was analyzed in this study with a variation of 25% to 100%. The physical properties of the MCFC, obtained from the literature [6,46] are listed in Table 2.

Table no 2. Characteristics of the MCFC components [6, 46]

Flowing length in electrolyte	$\delta = 0.0017 \text{ m}$	$a = 0.0294 \text{ m}$
	$A = 0.00005 \text{ m}^2$	$b = 3016 \text{ K}$
Oxidant utilization	$U_{ox} = 0.5$	
MCFC reference temperature	$T_0 = 923.15 \text{ K}$	

Figure 1a shows the schematic diagram of the hybrid system consisting of an indirect reforming molten carbonate fuel cell and a gas turbine as the main equipment and Figure 1b illustrates the hybrid system temperature-entropy plot depicted in Figure 1a.

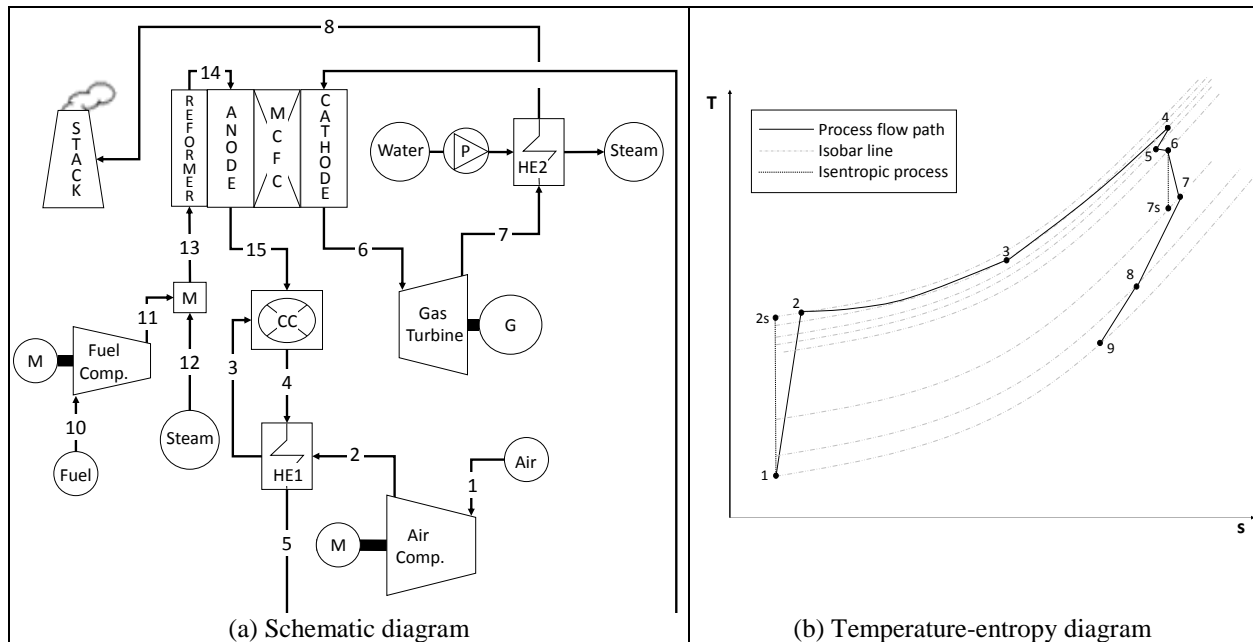


Figure no1. (a) Schematic diagram and (b) temperature-entropy plot of the hybrid system analyzed in this work.

The current density function of the MCFC, the anode and cathode resistance based on different pressure inputs, reforming rate, fuel utilization and the fuel cell operating temperature is analyzed in this paper. The performance of the fuel cell is also described as using the Nernst equation. Although it is possible to set MCFC fuel to use CO, this is not considered in this work.

Gas turbine in the hybrid system

The concept of using a gas turbine in a fuel cell integrated system is well-known for years. Research in the literature indicates that the concept was first analyzed by Ide et al. (1989), who compared three different hybrid systems in terms of net efficiency, energy generation, and energy recovery. The gas turbine modeling is based on Figure 1. The isentropic efficiency of the compressor is defined as [74]:

$$\eta_c = \frac{w_{c,s}}{w_c} = \frac{h_{2,s} - h_1}{h_2 - h_1} \quad (16)$$

Where: $w_{c,s}$ is the ideal (isentropic) specific compressor work (in SI units, kJ/kg); w_c is the specific compressor work (kJ/kg); $h_{2,s}$ is the specific enthalpy at the compressor exit (kJ/kg) in the isentropic process; h_2 is the specific enthalpy at the compressor exit (kJ/kg); h_1 is the specific enthalpy at the compressor inlet (kJ/kg).

The ideal temperature ($T_{2,s}$) of the working fluid at the compressor exit is determined using [74]:

$$\frac{T_{2,s}}{T_1} = \left(\frac{P_2}{P_1}\right)^{\frac{\gamma-1}{\gamma}} \quad (17)$$

Where: T_1 is the temperature at the compressor entrance (in SI units, K); P_2 and P_1 are the pressures at the compressor exit and entrance (Pa), respectively; γ is the ratio between specific heats at constant pressure (Cp) and constant volume (Cv). Applying the energy balance in the system, the work required for the compressor is [74]:

$$\dot{W}_C = \dot{m}_1(h_2 - h_1) \quad (18)$$

Where: \dot{W}_C is the compressor power (in SI units, kW) and \dot{m}_1 is the mass flowrate of the air (kg/s).

The first law of thermodynamics for the combustion chamber is expressed as [75]:

$$(\dot{m}_{air,FC} + \dot{m}_{fuel,FC}U_f) + \dot{m}_{fuel,FC}(1 - U_f) = \dot{m}_4 = \dot{m}_3 + \dot{m}_{15} \quad (19)$$

$$\dot{Q}_{comb} = \dot{m}_{fuel,FC}(1 - U_f)LHV \quad (20)$$

$$\dot{Q}_{loss} = \dot{m}_{fuel,FC}(1 - U_f)(1 - \eta_{comb})LHV \quad (21)$$

Where: U_f is the fuel utilization in the fuel cell; $\dot{m}_{air,FC}$ is the air mass flowrate of the fuel cell (kg/s); \dot{m}_3 and \dot{m}_{15} are the mass flowrate at the combustor entrance from the heat exchanger and the fuel cell anode, respectively; $\dot{m}_{fuel,FC}$ is the fuel mass flowrate of the fuel cell (kg/s); \dot{Q}_{comb} is the heat release in the combustion chamber (kW); LHV is the lower heating value of the fuel (kJ/kg); η_{comb} represents the combustor efficiency.

The entropy balance for the combustor is [75]:

$$\dot{m}_4s_4 + \frac{\dot{Q}_{comb}}{T_{comb}} + \dot{S}_{comb} - \dot{m}_3s_3 - \dot{m}_{15}s_{15} - \frac{\dot{Q}_{loss}}{T_\infty} = 0 \quad (22)$$

Where: T_{comb} is the adiabatic flame temperature (K); s_4 is the specific entropy (kJ/kg.K) at the combustor exit, s_3 and s_{15} is the specific entropy (kJ/kg.K) at the combustor entrance from the heat exchanger and fuel cell anode, respectively; \dot{S}_{comb} is the entropy generated in the combustion reaction (kW/K); \dot{Q}_{loss} is the heat transfer rate lost by the combustion chamber (kW); T_∞ is the ambient temperature (K).

The entropy generation rate inside the combustion chamber is [75]:

$$\dot{S}_{comb} = \dot{m}_3s_3 + \dot{m}_{15}s_{15} + \frac{\dot{Q}_{loss}}{T_\infty} - \left(\dot{m}_4s_4 + \frac{\dot{Q}_{comb}}{T_{comb}} \right) \quad (23)$$

The power demanded by the compressor (\dot{W}_C) is provided by the gas turbine (\dot{W}_{GT}). Therefore, the net power of the gas turbine system ($\dot{W}_{net,GT}$) is given by [76]:

$$\dot{W}_{net,GT} = \dot{W}_{GT} - \dot{W}_C \quad (24)$$

Knowing the turbine inlet temperature, the turbine exit temperature is calculated through the definition of isentropic efficiency (η_{GT}) of the turbine [76]:

$$\eta_{GT} = \frac{w_{GT}}{w_{GT,s}} = \frac{h_6 - h_7}{h_6 - h_{7,s}} \quad (25)$$

Where: $w_{GT,s}$ is the ideal (isentropic) specific gas turbine work (in SI units, kJ/kg); $h_{7,s}$ is the specific enthalpy at the gas turbine exit (kJ/kg) in the isentropic process; h_7 is the specific enthalpy at the gas turbine exit (kJ/kg); h_6 is the specific enthalpy at the gas turbine inlet (kJ/kg).

The gas turbine exit pressure (P_6) is [76]:

$$\frac{P_7}{P_6} = \left(\frac{T_{7,s}}{T_6} \right)^{\frac{\gamma}{\gamma-1}} \quad (26)$$

Where: $T_{7,s}$ is the ideal temperature of the working fluid at the gas turbine exit (K); T_6 is the temperature at the gas turbine entrance (K); P_6 is the gas turbine inlet pressure (Pa).

The entropy balance for the turbine is obtained as [76]:

$$\dot{m}_6s_6 - \dot{m}_7s_7 + \dot{S}_{GT} = 0 \quad (27)$$

From the mass conservation ($\dot{m}_6 = \dot{m}_7$). The entropy generation rate (\dot{S}_{GT}) during the expansion process is [75,77]:

$$\dot{S}_{GT} = \dot{m}_7(s_7 - s_6) \quad (28)$$

For the heat exchanger after the combustion chamber (HE1), its efficiency is described as [77]:

$$\eta_{HE1} = \frac{h_3 - h_2}{h_4 - h_5} \quad (29)$$

Besides, the entropy balance equation for the heat exchanger 1 is expressed as [77]:

$$\dot{m}_2s_2 - \dot{m}_3s_3 + \dot{m}_4s_4 - \dot{m}_5s_5 + \dot{S}_{HE1} = 0 \quad (30)$$

From the mass conservation ($\dot{m}_2 = \dot{m}_3$ and $\dot{m}_4 = \dot{m}_5$). Thus, the entropy generation rate inside the heat exchanger 1 (\dot{S}_{HE1}) is achieved with [75,77]:

$$\dot{S}_{HE1} = \dot{m}_2(s_3 - s_2) - \dot{m}_4(s_5 - s_4) \quad (31)$$

For the heat exchanger after the gas turbine (HE2), its efficiency is described as [77]:

$$\eta_{HE2} = \frac{h_{st} - h_w}{h_7 - h_8} \quad (32)$$

Where: h_{st} and h_w is the specific enthalpy (kJ/kg) of the steam and water, respectively.

The entropy balance equation for the heat exchanger 2 is expressed as [77]:

$$\dot{m}_7 s_7 - \dot{m}_8 s_8 + \dot{m}_w s_w - \dot{m}_{st} s_{st} + \dot{S}_{HE2} = 0 \quad (33)$$

From the mass conservation ($\dot{m}_7 = \dot{m}_8$ and $\dot{m}_w = \dot{m}_{st}$). Thus, the entropy generation rate inside the heat exchanger 2 (\dot{S}_{HE2}) is achieved with [75,77]:

$$\dot{S}_{HE} = \dot{m}_7 (s_8 - s_7) - \dot{m}_w (s_{st} - s_w) \quad (34)$$

Using the following energy balance equation, one may find the outlet temperature of the cycle [75,77]:

$$\dot{m}_7 (h_7 - h_8) = \dot{m}_w (h_{st} - h_w) \quad (35)$$

General balance for hybrid cycle

Figure 1 shows the MCFC / gas turbine hybrid system, which is analyzed as a single control volume. The mass balance of the hybrid system is [75]:

$$(\dot{m}_1 + \dot{m}_{10} + \dot{m}_{12}) - \dot{m}_8 = 0 \quad (36)$$

$$\dot{m}_1 = \dot{m}_2 = \dot{m}_3 \quad (37)$$

$$\dot{m}_{10} + \dot{m}_{12} = \dot{m}_{13} = \dot{m}_{14} = \dot{m}_{15} \quad (38)$$

$$(\dot{m}_{15} + \dot{m}_3) - \dot{m}_4 = 0 \quad (39)$$

$$\dot{m}_4 = \dot{m}_5 = \dot{m}_6 = \dot{m}_7 = \dot{m}_8 \quad (40)$$

On the other hand, the energy balance (first law) of the system is [75]:

$$\dot{m}_1 h_1 + \dot{m}_{fuel,FC} U_f LHV + \dot{m}_w h_w + \dot{Q}_{comb} - \dot{m}_8 h_8 - \dot{Q}_{loss} - \dot{W}_{FC,dc} - \dot{W}_{net,GT} = 0 \quad (41)$$

The total thermal yield of the plant is defined by the ratio between the net power and the total income power of the system [75]:

$$\eta_{tot} = \frac{\dot{W}_{net}}{\dot{Q}_{tot}} \quad (42)$$

$$\dot{W}_{net} = \dot{W}_{FC,ac} + \dot{W}_{gen} \quad (43)$$

$$\dot{W}_{FC,ac} = \eta_{inverter} \dot{W}_{FC,dc} \quad (44)$$

$$\dot{W}_{gen} = \eta_{gen} \dot{W}_{net,GT} \quad (45)$$

$$\dot{Q}_{tot} = \dot{m}_{fuel,FC} U_f LHV + \dot{Q}_{comb} \quad (46)$$

In which $\eta_{inverter}$ and η_{gen} are the inverter (DC to AC) and the electrical generator efficiency, respectively. Finally, the entropy generation rate within the system is the sum of entropy generated in all plant components [77]:

$$S_{sys} = \sum_i S_i \quad (47)$$

Where i stands for the hybrid cycle equipment (compressor, heat exchanger, MCFC, combustor and gas turbine).

III. RESULTS AND DISCUSSION

The main input parameters of each component of the hybrid system are listed in Table 3. The considerations taken into account were that the equipment is in steady-state, without losses, in the electrical generator connected to the fuel cell output.

Table no 3. Equipment entry parameters [69]

Name	Parameters
Fuel source	Methane (CH ₄): 100%. Lower heating value of 50006 kJ/kg; Pressure of 101325 Pa and temperature of 288.15 K. Mass flow rate of 0.05 kg/s.
Air source and ambient conditions	N ₂ : 77.29%, O ₂ : 20.75%, H ₂ O: 1.01%, CO ₂ : 0.03% and Ar: 0.92%; Pressure of 101325 Pa and temperature of 288.15 K. Relative humidity of 60%
Air and Fuel Compressor	Isentropic efficiency of 1.00; Mechanical efficiency of 1.00; Pressure ratio ranging from 3 to 6.
Turbine	Isentropic efficiency of 0.80; Mechanical efficiency of 1.00
Electrical generator	Efficiency of 0.98
Heat exchanger	Pressure drop in hot and cold side of 10%; Effectiveness of 0.92
Stack	Exhaust Pressure of 101325 Pa

The results for the ohmic polarization of the MCFC for the anode (a) and the cathode (b) are presented in Figure 2. The obtained values derived from Nernst equation as a function of the operating pressure, steam/carbon ratio varying from 2 to 3 and fuel utilization in the anode (U_{fan}) ranging from 0.25 to 1.00 considering the temperature of 923.15 K.

The results show that the resistance in the electrodes decreases exponentially with increasing pressure and the steam/carbon (S/C) ratio, followed by the fuel utilization in the anode. This was expected based on: (i) the higher the S/C ratio, the greater the conversion of the fuel to H_2 , favoring an increase in the availability in the anode and reducing the concentration resistance; (ii) higher rate of fuel utilization also implies higher activity on this electrode; (ii) the increase of the pressure favors the availability of H_2 at the catalyst sites, besides promoting the diffusibility of the ions by the electrolyte after the reaction at the electrode, releasing the sites so that the reaction occurs at higher rates.

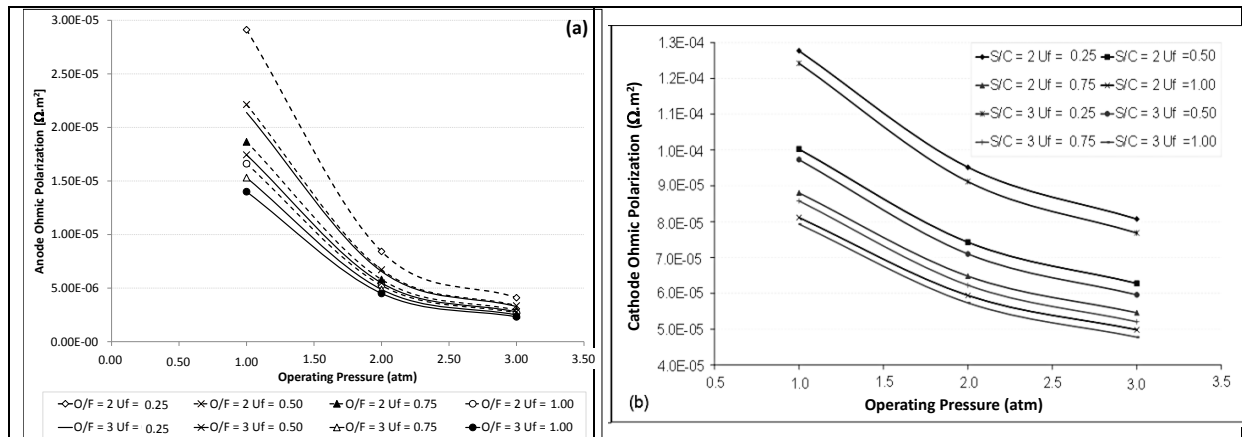


Figure no2. Results for ohmic polarization in the anode (a) and cathode (b) as a function of the pressure and steam to carbon ratio (S/C) for the operating temperature of 923.15 K.

The reduction in resistance in the electrodes will imply in a smaller reduction in the operating voltage of the cell and, in turn, in a higher power density. These results confirm with that described by [6], which emphasizes that the increase in operating pressure results in increased fuel cell voltage due to the increased solubility of gases and increased mass transport due to the increase in the partial pressures of the gases.

Regarding the influence of the fuel cell operating temperature on the resistance, already demonstrated by Leal [58], the results obtained are expressed in Figure 3, for which the total resistance of the cell was given as a function of the temperature (ranging from 773.15 K to 973.15 K) at different pressures.

It is possible to observe that the temperature has a greater influence on the resistance of the fuel cell than the operating pressure. With these results, it was possible to find the points of greatest energy production by the fuel cell, shown in Figure 4. These results were used to calculate the power produced by the hybrid system in MS Excel software. The parameters obtained and used for the fuel cell model was its operating temperature and pressure, current density, output voltage, fuel and oxidant utilization, and the internal reforming rate.

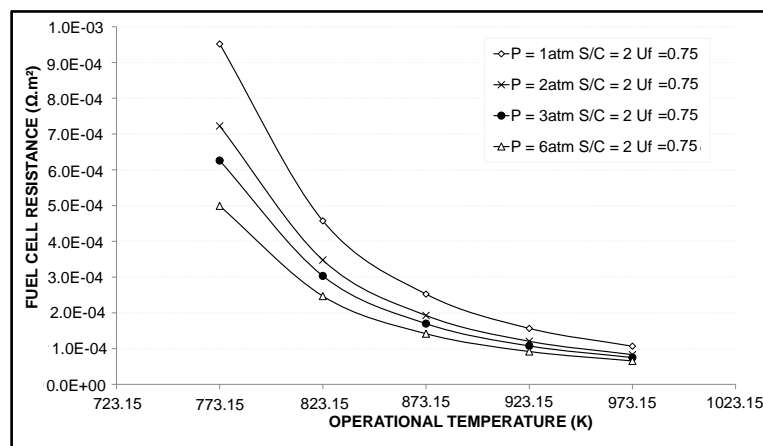


Figure no 3. Results of the fuel cell resistance as a function of the operating temperature (773.15 K ≤ T ≤ 973.15 K), and pressure (from 1 atm to 6 atm), for steam-to-carbon ratio of 2.0 and fuel utilization of 0.75

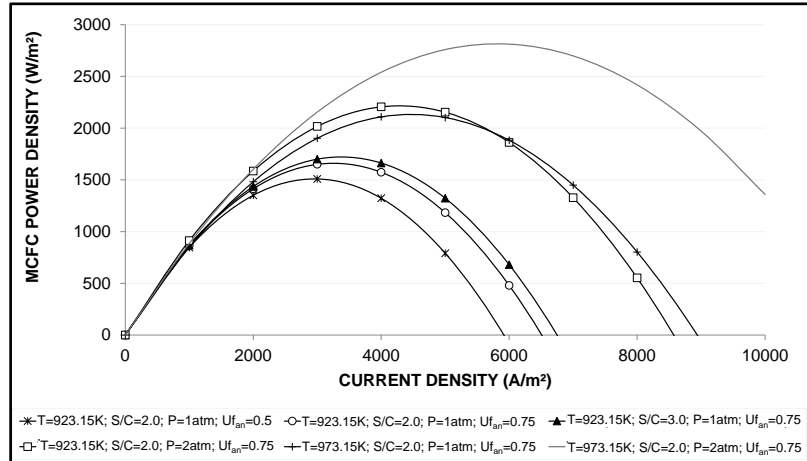


Figure no4. Results of the fuel cell power density as a function of the current density ($0 \text{ A/m}^2 \leq j \leq 10000 \text{ A/m}^2$), operating pressure (1 and 2 atm), fuel utilization of 0.50 and 0.75, and steam to carbon ratio of 2.0 and 3.0.

As shown in the results of the total resistance (Figure 3), the increase in pressure and in the operating temperature of the fuel cell results in significant increases in the power production (Figure 4), being the association between these two parameters. It can also be verified, according to Figure 4, a parabolic behavior of the relationship between power and current density, and for higher temperatures, the higher the power limit will be. For the temperature of 973.15 K, at a pressure of 1 atm; U_{fan} of 0.75 and S/C ratio of 2, the power reached a maximum value of 2108 W/m^2 at 4000 A/m^2 , while for the temperature of 923.15 K a power output reached 1509 W/m^2 at 3000 A/m^2 . This means an increase of 39.7% in power density and 33.3% in the peak current density for a 7.7% change in temperature. In addition, for the temperature of 923.15 K and current density of 4000 A/m^2 , the variation in the fuel utilization resulted in the increase of 19.0% (at 1 atm pressure and S/C ratio of 2) and 15.1% (at 1 atm pressure and S/C ratio of 3). The pressure increase from 1 to 2 atm resulted in increases of up to 40.2% (U_{fan} of 0.75 and S/C ratio of 2), while the increase in the S/C ratio increased by 9.2%, at pressure of 1 atm and U_{fan} of 0.5, 5.7%, at a pressure of 1 atm and U_{fan} of 0.75.

The hybrid system was built and the points of greatest energy production by the fuel cell were inserted in the configuration to evaluate the influence of these parameters on the complete hybrid system. Although the reforming reactions could be calculated directly through MCFC apparatus, the mass fractions at anode inlet were easier to control using an indirect internal reformer. Figure 5 shows the results for power delivered and net delivered power efficiency as a function of operating pressure from 3atm to 6 atm, the temperature of 923.15 K and 973.15 K, fuel utilization of 0.75, and steam to carbon of 2.

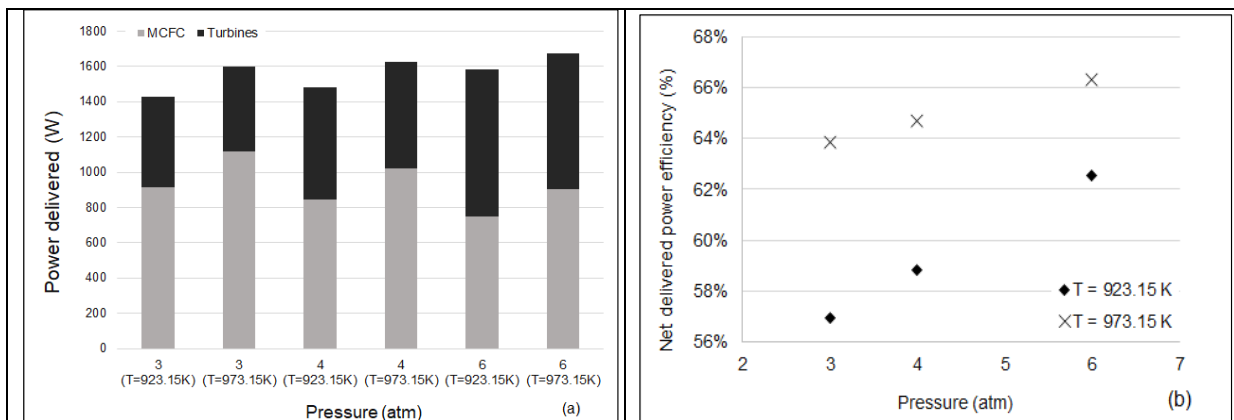


Figure no 5. Results of power delivered (a) and net delivered power efficiency (b) as a function of pressure ($3 \text{ atm} \leq P \leq 6 \text{ atm}$), temperature of 923.15 K and 973.15 K for fuel utilization of 0.75 and steam to carbon of 2.

Figure 5 relates the delivered power to the pressure variation for temperatures of 923.15 K and 973.15 K. For the same fuel mass flowrate in the system, it is possible to observe that the variation in the operating temperature of the fuel cell resulted in a greater increase in the total power of the hybrid system when compared to the results of the pressure increase. The increase in temperature from 923.15 K to 973.15 K

resulted in a maximum increase of 12% in the delivered power and corresponding to a 6.95% system efficiency increase, demonstrated in Figure 5(b). This effect was a consequence of an increase in the delivered power of the fuel cell, already expected and described with the individual modeling of the device.

An increase in pressure from 3 to 4 atm resulted in a maximum increase of 3.86% in delivered power, corresponding to an increase of 2.22% system efficiency (T = 923.15 K). This is because, although an increase in the fuel cell's power density was observed for the same mass flow rate in the system, the pressure negatively influenced the value of the total delivered power of the fuel cell. For this pressure variation, there was a reduction of 7.79% in the delivered power of the MCFC, although the delivered power of the gas turbine increased by 24.7%, also showing a higher effect of the pressure on the turbine operation regarding the working fluid temperature. Results of turbines and MCFC power delivered for a variation in steam to carbon ratio, operating temperature, fuel utilization variation, are shown in Figure 6.

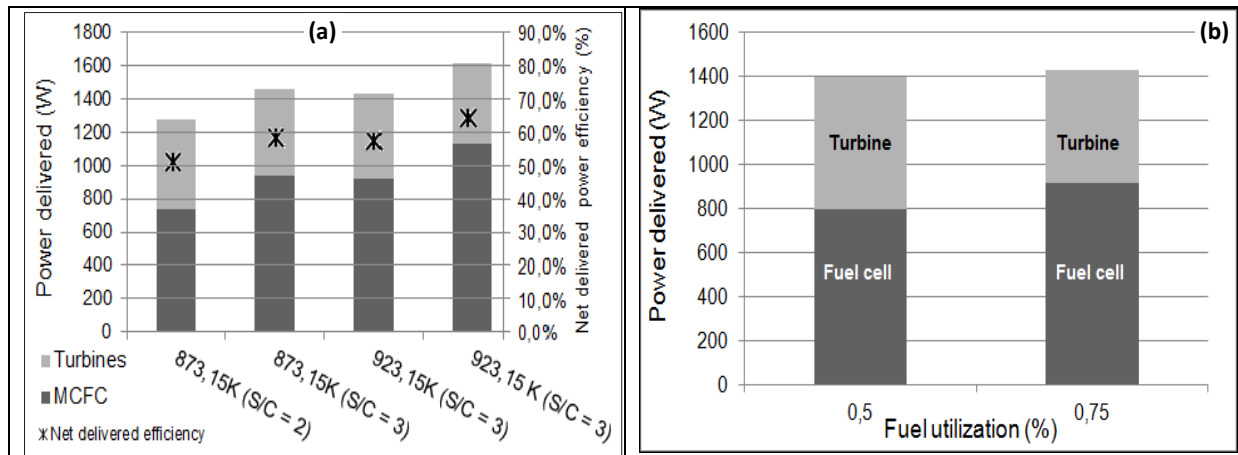


Figure no6. Results of the power delivered and efficiency of each main component as a function of the operating temperature and steam to carbon ratio (a), and the fuel utilization with temperature of 923.15 K, both in the pressure of 3 atm.

Results presented in Figure 6a and 6b indicate that the variation in the reform rate from 2 to 3 promoted an increase in the power delivered by the MCFC for both temperatures of 873.15 K and 923.15 K compared (27.11% and 23.0%, respectively). On the other hand, this increase resulted in a reduction in power delivered by the gas turbine, with a reduction of 4.5% for the temperature of 873.15 K and 6.0% for the temperature of 923.15 K. Nevertheless, there was an increase in total delivered power and in the system's network efficiency. For 873.15 K, an increase of 13.7% in the delivered power and 7.0% in the network efficiency was observed, and at 923.15 K, 13.0% and 7.17%, respectively.

In turn, it was possible to conclude that the variation in the fuel utilization rate from 0.50 to 0.75 also promoted a 14.5% increase in the power delivered by the MCFC to the system studied at a temperature of 923.15 K and a pressure of 3atm. As for the steam-to-carbon ratio, this increase resulted in a reduction in the power delivered by the turbine pair by 14% in the delivered power. The result was expected, given that the increase in fuel utilization by the cell reduces the availability of fuel to be used in generating turbine power. The result was a slight increase in power and total delivered network efficiency (2.3% and 2.4%, respectively).

IV.CONCLUSIONS

It becomes clear that, in the design point, the fuel cell is the main energy generator, while the turbine is the second power generation equipment. It was also possible to conclude that, for the hybrid system, the increase in fuel cell operating temperature and fuel reform promoted an increase in fuel cell and system delivered power, although the increase in temperature did not significantly influence the power delivered by the turbine and the reform rate has resulted in a decrease of this. The increase in pressure, on the other hand, resulted in an increase in the power delivered by the gas turbine and in a decrease of the power delivered by the fuel cell, maintaining the same fuel mass flow rate. However, the power density of the fuel cell, in this case, increases. Moreover, both the increase in the fuel cell's operating temperature and in the pressure and reform rate culminated in an increase in the efficiency of the hybrid system. The variation in the rate of fuel utilization by the fuel cell, on the other hand, did not show an expressive increase in the efficiency of the system or in the total delivered power, since the increase in energy production by the cell was affected by the reduction of energy production by the turbines.

Further research is needed to check the influence of the studied parameters on carbon deposition in the MCFC and evaluation of its lifetime for economic analysis of the increase of these variables in the system.

ACKNOWLEDGMENTS

The authors acknowledge FAPEMIG (Foundation for Research Support of Minas Gerais State) award number APQ-02156-14, the Federal University of Ouro Preto (UFOP) and Gorceix Foundation for the financial support to this work. Also, thanks for those who helped in the execution of this research project.

REFERENCES

- [1] ENERDATA, Global Energy Statistical Yearbook 2019. Available at <https://www.enerdata.net/publications/reports-presentations/world-energy-trends.html>. Accessed on 01/13/2020.
- [2] Dincer, I., Rosen, M.A., Ahmadi, P. (2017). Optimization of Energy Systems. United Kingdom: John Wiley & Sons Ltd., 2017. DOI: 10.1002/9781118894484
- [3] Hauschild, L. (2006). Evaluation of Operation Strategies of Hybrid Photovoltaic-Wind-Diesel Systems. São Paulo: Master's dissertation in Energy, University of São Paulo (Graduate Program in Energy), 117 pages. (In Portuguese).
- [4] McLarty, D., Brouwer, J., Samuelsen, S. (2014). Fuel cell–gas turbine hybrid system design part I: Steady state performance. *J Power Sources* 257, pp. 412-20. <https://doi.org/10.1016/j.jpowsour.2013.11.122>
- [5] McLarty, D., Brouwer, J., Samuelsen, S. (2014). Fuel cell–gas turbine hybrid system design part II: Dynamics and control. *J Power Sources* 254, pp. 126-36. <https://doi.org/10.1016/j.jpowsour.2013.11.123>
- [6] EG&G Technical Services, Inc. (2004). Fuel cell handbook. 7th ed. Contract No. DE-AM26-99FT40575. U.S. Department of Energy, Office of Fossil Energy, National Energy Technology Laboratory. Available at <https://www.netl.doe.gov/sites/default/files/netl-file/FCHandbook7.pdf>. Accessed on 01/13/2020.
- [7] Larminie, J., Dicks, A. (2003). Fuel Cells Explained, 2nd Ed., John Wiley and. Sons.
- [8] Beér, J. M. (2007). High efficiency electric power generation: the environmental role. *Prog Energy Comb Sci*, 33, pp. 107-134. <https://doi.org/10.1016/j.pecs.2006.08.002>
- [9] Naidja, A., Krishna, C.R., Butcher, T., Mahajan, D. (2003). Cool flame partial oxidation and its role in combustion and reforming of fuels for fuel cell systems. *Prog Energy Comb Science* 29, pp. 155-191. [https://doi.org/10.1016/S0360-1285\(03\)00018-2](https://doi.org/10.1016/S0360-1285(03)00018-2)
- [10] Freni, S. (2001). Rh based catalysts for indirect internal reforming ethanol applications in molten carbonate fuel cells. *J Power Sources* 94, pp. 14-19. [https://doi.org/10.1016/S0378-7753\(00\)00593-0](https://doi.org/10.1016/S0378-7753(00)00593-0)
- [11] Richards, G.A., Mcmillian, M.M., Gemmen, R.S., Rogers, W.A., Cully, S.R. (2001). Issues for low-emission, fuel-flexible power systems. *Prog Energy Comb Science* 27, pp. 141-69. [https://doi.org/10.1016/S0360-1285\(00\)00019-8](https://doi.org/10.1016/S0360-1285(00)00019-8)
- [12] Aravind, P.V., Jong, W. (2012). Evaluation of high temperature gas cleaning options for biomass gasification product gas for solid oxide fuel cells. *Prog Energy Comb Science* 38, pp. 737-764. <https://doi.org/10.1016/j.pecs.2012.03.006>
- [13] Marefati, M., Mehrpooya, M. (2019). Introducing and investigation of a combined molten carbonate fuel cell, thermoelectric generator, linear fresnel solar reflector and power turbine combined heating and power process. *Journal of Cleaner Production* 240, p. 118247. <https://doi.org/10.1016/j.jclepro.2019.118247>.
- [14] Marefati, M., Mehrpooya, M., Shafii, M.B. (2019). A hybrid molten carbonate fuel cell and parabolic trough solar collector, combined heating and power plant with carbon dioxide capturing process. *En Conv Manag* 183, pp. 193-209. <https://doi.org/10.1016/j.enconman.2019.01.002>
- [15] Mehrpooya, M., Ghorbani, B., Moradi, M. (2019). A novel MCFC hybrid power generation process using solar parabolic dish thermal energy. *Int J Hyd Energy* 44(16), pp. 8548-8565. <https://doi.org/10.1016/j.ijhydene.2018.12.014>.
- [16] Mahmoudi, S.M.S., Ghavimi, A.R., Yari, M. (2019). Two objective optimization for a new molten carbonate fuel cell based power producing system. *App Therm Engin* 155, pp. 313-330. <https://doi.org/10.1016/j.applthermaleng.2019.03.153>.
- [17] Sadeghi, S., Askari, I.B. (2019). Prefeasibility techno-economic assessment of a hybrid power plant with photovoltaic, fuel cell and Compressed Air Energy Storage (CAES). *Energy* 168, pp. 409-424. <https://doi.org/10.1016/j.energy.2018.11.108>.
- [18] Hosseini, S.S., Mehrpooya, M., Alsagri, A.S., Alrobaian, A.A. (2019). Introducing, evaluation and exergetic performance assessment of a novel hybrid system composed of MCFC, methanol synthesis process, and a combined power cycle. *En Conv Manag* 197, p. 111878. <https://doi.org/10.1016/j.enconman.2019.111878>.
- [19] Erzen, S., Açıkkalp, E., Hepbasli, A. (2019). Performance assessment of a biogas fuelled molten carbonate fuel cell-thermophotovoltaic cell-thermally regenerative electrochemical cycle-absorption refrigerator-

- alkaline electrolyzer for multigenerational applications. *Int J Hydr Energy* 44(42), pp. 23741-23749. <https://doi.org/10.1016/j.ijhydene.2019.07.057>.
- [20] Ghorbani, B., Mehrpooya, M., Mousavi, S.A. (2019). Hybrid molten carbonate fuel cell power plant and multiple-effect desalination system. *J Clean Prod* 220, pp.1039-1051. <https://doi.org/10.1016/j.jclepro.2019.02.215>
- [21] Ghorbani, B., Shirmohammadi, R., Mehrpooya, M., Mafi, M. (2018). Applying an integrated trigeneration incorporating hybrid energy systems for natural gas liquefaction. *Energy* 149, pp. 848-64. <https://doi.org/10.1016/j.energy.2018.02.093>
- [22] Ansarinasab, H., Mehrpooya, M. (2018). Investigation of a combined molten carbonate fuel cell, gas turbine and Stirling engine combined cooling heating and power (CCHP) process by exergy cost sensitivity analysis. *En Conv Manag* 165, pp. 291-303. <https://doi.org/10.1016/j.enconman.2018.03.067>
- [23] Ahn, J., Park, S.H., Lee, S., Noh, Y., Chang, D. (2018). Molten carbonate fuel cell (MCFC)-based hybrid propulsion systems for a liquefied hydrogen tanker. *Int J Hydrogen Energy*, 43(15), pp. 7525-37. <https://doi.org/10.1016/j.ijhydene.2018.03.015>
- [24] Duan, L., Lu, H., Yuan, M., Lv, Z. (2018). Optimization and part-load performance analysis of MCFC/ST hybrid power system. *Energy* 152, pp. 682-693. <https://doi.org/10.1016/j.energy.2018.03.178>
- [25] Ahmadi, M.H., Jokar, M.A., Ming, T., Feidt, M., Astaraei, F.R. (2018). Multi-objective performance optimization of irreversible molten carbonate fuel cell–Braysson heat engine and thermodynamic analysis with ecological objective approach. *Energy* 144, pp. 707-722. <https://doi.org/10.1016/j.energy.2017.12.028>
- [26] Ahn, J., Noh, Y., Park, S.H., Choi, B.I., Chang, D. (2017). Fuzzy-based failure mode and effect analysis (FMEA) of a hybrid molten carbonate fuel cell (MCFC) and gas turbine system for marine propulsion. *J Power Sources* 364, pp. 226-33. <https://doi.org/10.1016/j.jpowsour.2017.08.028>
- [27] Mehrpooya, M., Sayyad, S., Zonouz, M.J. (2017). Energy, exergy and sensitivity analyses of a hybrid combined cooling, heating and power (CCHP) plant with molten carbonate fuel cell (MCFC) and Stirling engine. *J Cleaner Prod* 148, pp. 283-94. <https://doi.org/10.1016/j.jclepro.2017.01.157>
- [28] Açikkalp, E. (2017). Ecologic and sustainable objective thermodynamic evaluation of molten carbonate fuel cell–supercritical CO₂ Brayton cycle hybrid system. *Int J Hydrogen Energy* 42(9), pp. 6272-80. <https://doi.org/10.1016/j.ijhydene.2016.12.110>
- [29] Açikkalp, E. (2017). Performance analysis of irreversible molten carbonate fuel cell – Braysson heat engine with ecological objective approach. *En Conv Manag* 132, pp. 432-37. <https://doi.org/10.1016/j.enconman.2016.11.042>
- [30] Jokar, M.A., Ahmadi, M.H., Sharifpur, M., Meyer, J.P., Ming, T. (2017). Thermodynamic evaluation and multi-objective optimization of molten carbonate fuel cell-supercritical CO₂ Brayton cycle hybrid system. *En Conv Manag*, 153, pp. 538-56. <https://doi.org/10.1016/j.enconman.2017.10.027>
- [31] Mehrpooya, M., Rahbari, C., Moosavian, S.M.A. (2017). Introducing a hybrid multi-generation fuel cell system, hydrogen production and cryogenic CO₂ capturing process. *Chem Eng Proces - Proc Intens* 120, pp. 134-47. <https://doi.org/10.1016/j.cep.2017.07.008>
- [32] Mehrpooya, M., Ansarinasab, H., Sharifzadeh, M.M.M., Rosen, M.A. (2017). Process development and exergy cost sensitivity analysis of a hybrid molten carbonate fuel cell power plant and carbon dioxide capturing process. *J Power Sources* 364, pp. 299-315. <https://doi.org/10.1016/j.jpowsour.2017.08.024>
- [33] Zhang, H., Chen, B., Xu, H., Ni, M. (2016). Thermodynamic assessment of an integrated molten carbonate fuel cell and absorption refrigerator hybrid system for combined power and cooling applications. *Int J Refrigeration* 70, pp. 1-12. <https://doi.org/10.1016/j.ijrefrig.2016.07.011>
- [34] Yang, Z., Liao, T., Zhou, Y., Lin, G., Chen, J. (2016). Performance evaluation and parametric optimum design of a molten carbonate fuel cell-thermophotovoltaic cell hybrid system. *En Conv Manag* 128, pp. 28-33. <https://doi.org/10.1016/j.enconman.2016.09.051>
- [35] Duan, L., Yue, L., Feng, T., Lu, H., Bian, J. (2016). Study on a novel pressurized MCFC hybrid system with CO₂ capture. *Energy* 109, pp. 737-50. <https://doi.org/10.1016/j.energy.2016.05.074>
- [36] Duan, L., Yue, L., Qu, W., Yang, Y. (2015). Study on CO₂ capture from molten carbonate fuel cell hybrid system integrated with oxygen ion transfer membrane. *Energy* 93, pp. 20-30. <https://doi.org/10.1016/j.energy.2015.07.137>
- [37] Zhang, X., Liu, H., Ni, M., Chen, J. (2015) Performance evaluation and parametric optimum design of a syngas molten carbonate fuel cell and gas turbine hybrid system. *Renew Energy* 80 407-414. <https://doi.org/10.1016/j.renene.2015.02.035>
- [38] Mamaghani, A.H., Najafi, B., Shirazi, A., Rinaldi, F. (2015) Exergetic, economic, and environmental evaluations and multi-objective optimization of a combined molten carbonate fuel cell-gas turbine system. *App Thermal Eng* 77 1-11. <https://doi.org/10.1016/j.applthermaleng.2014.12.016>

- [39] Yazdanfar, J., Mehrpooya, M., Yousefi, H., Palizdar, A. (2015). Energy and exergy analysis and optimal design of the hybrid molten carbonate fuel cell power plant and carbon dioxide capturing process. *En Conv Manag* 98 15-27. <https://doi.org/10.1016/j.enconman.2015.03.076>
- [40] Roberts, R., Brouwer, J. (2006) Dynamic simulation of a pressurized 220 kW solid oxide fuel cell – gas turbine hybrid system: modeled performance compared to measured results. *J. Fuel Cell Sci. Technol.* 3(1), pp.18-25. <https://doi.org/10.1115/1.2133802>
- [41] FUELCELL ENERGY INC. (2006). Investor Relations Newsletter.
- [42] EURELECTRIC. (2003). Efficiency in Electricity Generation. Brussels, Belgium. Available at https://www.vgb.org/en/data_powergeneration.html?dfid=14494.
- [43] Yoshida, F., Ono, N., Izaki, Y., Watanabe, T., Abe, T. (1998). Numerical Analyses of the Internal Conditions of a Molten Carbonate Fuel Cell Stack: Comparison of Stack Performances for Various Gas Flow Types. *J Power Sources* 71(1-2), pp. 328-336. [https://doi.org/10.1016/S0378-7753\(97\)02727-4](https://doi.org/10.1016/S0378-7753(97)02727-4)
- [44] Bosio, B., Costamagna, P., Parodi, F. (1999) Modelling and Experimentation of Molten Carbonate Fuel Cell Reactors in a Scale-up Process. *Chem Engin Sci*, 54(13–14), pp. 2907-2916. [https://doi.org/10.1016/S0009-2509\(98\)00414-X](https://doi.org/10.1016/S0009-2509(98)00414-X)
- [45] Koh, J.H., Kang, B.S., Lim, H.C. (2000). Effect of Various Stack Parameters on Temperature Rise in Molten Carbonate Fuel Cell Stack Operation. *J Pow Sourc* 91(2), pp. 161-171. [https://doi.org/10.1016/S0378-7753\(00\)00463-8](https://doi.org/10.1016/S0378-7753(00)00463-8)
- [46] Zhang, X., Wang, Y., Guo, J., Shih, T-M., Chen, J. (2014). A unified model of high-temperature fuel-cell heat engine hybrid systems and analyses of its optimum performances. *Int J Hydr Energy*, pp. 1811-1825. <https://doi.org/10.1016/j.ijhydene.2013.11.027>
- [47] Shipley, A.M., Elliott, R.N. (2004). Stationary fuel cells: future promise, current hype. *Fuel Cells ACEEE*. Washington, D. C: American Council for an Energy-Efficient Economy.
- [48] Pashchenko, D. (2018). Energy optimization analysis of a thermochemical exhaust gas recuperation system of a gas turbine unit. *Energy Conversion and Management* 171:917–24. <https://doi.org/10.1016/j.enconman.2018.06.057>
- [49] Mclarty, D., Kuniba, Y., Brouwer, J., Samuelsen, S. (2012). Experimental and theoretical evidence for control requirements in solid oxide fuel cell gas turbine hybrid systems. *J Power Sources* 209, pp. 195-203. <https://doi.org/10.1016/j.jpowsour.2012.02.102>
- [50] Yu, L.J., Ren, G.P., Jiang, X.M., Yuan, J.Q., Cao, G.Y. (2007). Experiment and numerical simulation on the performance of a kw-scale molten carbonate fuel cell stack. *Braz. J. Chem. Eng.*, 24(4), pp. 523-533. <http://dx.doi.org/10.1590/S0104-66322007000400006>
- [51] Yu, L.J., Ren, G.P., Jiang, X.M., Yuan, J.Q., Cao, G.Y. (2007). Experiment and numerical simulation on the performance of a kw-scale molten carbonate fuel cell stack. *Braz J Chem Eng* 24(4), pp. 523-533. <http://dx.doi.org/10.1590/S0104-66322007000400006>
- [52] Williams, M.C., Strakey, J.P., Singhal, S.C. (2004). U.S. Distributed Generation Fuel Cell Program. *J. Power Sources* 131(1-2), pp. 79-85. <https://doi.org/10.1016/j.jpowsour.2004.01.021>
- [53] FUELCELLTODAY. (2013). The fuel cell industry review. Available at: <http://www.fuelcelltoday.com/>.
- [54] Sundmacher, K., Kienle, A., Pesch, H.J., Berndt, J.F., Hauppmann, G. *Molten Carbonate Fuel Cells Modeling, Analysis, Simulation and Control*. Wiley. 2007. DOI: 10.1002/9783527611324
- [55] Chan, S.H., Khor, K.A., Xia, Z.T. (2001). A complete polarization model of a solid oxide fuel cell and its sensitivity to the change of cell component thickness. *J Pow Sourc* 93, pp. 130-140. [https://doi.org/10.1016/S0378-7753\(00\)00556-5](https://doi.org/10.1016/S0378-7753(00)00556-5)
- [56] Chan, S.H., Low, C.F., Ding, O.L. (2002). Energy and exergy analysis of simple solid-oxide fuel-cell power systems. *J Pow Sourc* 103(2), pp. 188-200. [https://doi.org/10.1016/S0378-7753\(01\)00842-4](https://doi.org/10.1016/S0378-7753(01)00842-4)
- [57] Brouwer, J., Jabbari, F., Leal, E. M., Orr, T. (2006) Analysis of a molten carbonate fuel cell: Numerical modeling and experimental validation. *J Pow Sourc* 158(1), pp. 213-224. <https://doi.org/10.1016/j.jpowsour.2005.07.093>
- [58] Leal, E.M. Characterization of cogeneration systems using fuel cells. Ph.D. dissertation (Mechanical Engineering). São Paulo State University. 191 pages, 2003. (In Portuguese).
- [59] Wee, J-H. Molten carbonate fuel cell and gas turbine hybrid systems as distributed energy resources. *Applied Energy*, 88(12) (2011) 4252-63. <https://doi.org/10.1016/j.apenergy.2011.05.043>
- [60] Liese, E.A., Gemmen, R.S., Jabbari, F., Brouwer, J. (1999). Technical development issues and dynamic modeling of gas turbine and fuel cell hybrid systems. ASME paper 99-GT-360. <https://doi.org/10.1115/99-GT-360>
- [61] Leeper, J. D. (1999). The hybrid cycle: integration of a fuel cell with a gas turbine. ASME paper 99-GT-430. <https://doi.org/10.1115/99-GT-430>

- [62] Massardo, A.F., McDonald, C.F., Korakianitis, T. (2000). Microturbine/fuel cell coupling for high efficiency electrical power generation. In: Proceedings of ASME TurboExpo, Munich. <https://doi.org/10.1115/1.1398552>
- [63] Gemmen, R.S., Liese, E.A., Rivera, J.G., Jabbari, F., Brouwer, J. (2000). Development of dynamic modeling tools for solid oxide and molten carbonate hybrid fuel cell gas turbine systems. In: Proceedings of ASME TurboExpo, Munich. <https://doi.org/10.1115/2000-GT-0554>
- [64] Lunghi, P., Bove, E., Desideri, U. (2003). Analysis and optimization of hybrid MCFC gas turbine plants. *J Pow Sourc* 118, pp. 108-117. [https://doi.org/10.1016/S0378-7753\(03\)00068-5](https://doi.org/10.1016/S0378-7753(03)00068-5)
- [65] Lobachyov, K.V., Richter, H.J. (1997). Addition of highly efficient bottoming cycles for the nth-generation molten carbonate fuel cell power plant. *J Energy Resour Technol* 119(2), pp. 103-108. doi: <https://doi.org/10.1115/1.2794972>
- [66] Jurado, F. (2000). Study of molten carbonate fuel cell-microturbine hybrid power cycles. *J Pow Sourc* 111, pp. 121-129. [https://doi.org/10.1016/S0378-7753\(02\)00340-3](https://doi.org/10.1016/S0378-7753(02)00340-3)
- [67] Grillo, O., Magistri, L., Massardo, A.F. (2003). Hybrid system for distributed power generation based on pressurisation and heat recovering of an existing 100 kW molten carbonate fuel cell. *J Pow Sourc* 115(2), pp. 252-267. [https://doi.org/10.1016/S0378-7753\(02\)00730-9](https://doi.org/10.1016/S0378-7753(02)00730-9)
- [68] Xu, J., Froment, G.F. (1989). Methane Steam Reforming, Methanation and Water-Gas Shift: 1. Intrinsic Kinetics. *AIChE Journal* 35(1), pp. 88-96. <https://doi.org/10.1002/aic.690350109>
- [69] Barmaki, R. Thermodynamic analysis of solid oxide fuel cell hybrid power plant and gas turbine. In: IEEE 3rd Conference on Thermal Power Plants. 2011. Available at https://www.researchgate.net/publication/273445344_Thermodynamic_analysis_of_solid_oxide_fuel_cell_hybrid_power_plant_and_gas_turbine. Accessed on 02/16/2019.
- [70] Azizi, M.A., Brouwer, J. (2018). Progress in solid oxide fuel cell-gas turbine hybrid power systems: System design and analysis, transient operation, controls and optimization. *App En* 215, pp. 237-89. <https://doi.org/10.1016/j.apenergy.2018.01.098>
- [71] Pashchenko, D. (2019). Experimental investigation of synthesis gas production by methane reforming with flue gas over a NiO-Al₂O₃ catalyst: Reforming characteristics and pressure drop. *Int J Hydrogen Energy*, 44(14): 7073-82. <https://doi.org/10.1016/j.ijhydene.2019.01.250>
- [72] Pashchenko, D. (2018). First law energy analysis of thermochemical waste-heat recuperation by steam methane reforming. *Energy* 2018; 143:478-87. <https://doi.org/10.1016/j.energy.2017.11.012>
- [73] Pashchenko, D. (2019). Flow dynamic in a packed bed filled with Ni-Al₂O₃ porous catalyst: experimental and numerical approach. *Reaction Engineering, Kinetics and Catalysis. AIChE Journal* 2019; 65(5):e16558. <https://doi.org/10.1002/aic.16558>
- [74] Bejan, A., Moran, M.J. (1996). Thermal design and optimization. New York: John Wiley&Sons.
- [75] Welaya, Y.M.A., Mosleh, M., Ammar, N.R. (2013). Thermodynamic analysis of a combined gas turbine power plant with a solid oxide fuel cell for marine applications. *Int J Naval Archit Ocean Eng.* 5(4):529-45. <https://doi.org/10.2478/IJNAOE-2013-0151>
- [76] Cohen, H., Rogers, G.F.C., Saravanamuttoo, H.I.H. (1996). Gas Turbine Theory. 4th ed. Harlow: Longman.
- [77] Cengel, Y.A., Boles, M.A. (2015). Thermodynamics: an Engineering Approach. 8th ed. New York: McGraw-Hill Education.

Elisângela Martins Leal et al. "Analysis of a Hybrid Molten Carbonate Fuel Cell and Gas Turbine Cycle." *IOSR Journal of Engineering (IOSRJEN)*, 10(3), 2020, pp. 01-14.